

PAPER

Numerical simulation and experiment of error field measurement using luminous trace of electron beam in SST-1

To cite this article: Someswar DUTTA et al 2019 *Plasma Sci. Technol.* **21** 105101

View the [article online](#) for updates and enhancements.

You may also like

- [Development and Integration of a Data Acquisition System for SST-1 Phase-1 Plasma Diagnostics](#)
Amit K Srivastava, Manika Sharma, Imran Mansuri et al.

- [Test results on systems developed for the SST-1 tokamak](#)
D. Bora and SST-1 Team

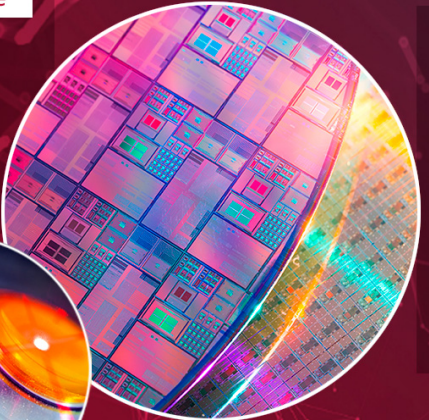
- [Spin splitting in monoperiodic systems described by magnetic line groups](#)
Sergei A Egorov, Daniel B Litvin, Andrei V Bandura et al.



Analysis Solutions for your **Plasma Research**

For Surface Science

- Surface Analysis
- SIMS
- 3D depth Profiling
- Nanometre depth resolution



Click to view our product catalogue

For Plasma Diagnostics

- Plasma characterisation
- Customised systems to suit plasma Configuration
- Mass and energy analysis of plasma ions
- Characterisation of neutrals and radicals



■ Knowledge ■ Experience ■ Expertise

Contact Hiden Analytical for further details:

W www.HidenAnalytical.com
E info@hiden.co.uk

This content was downloaded from IP address 103.49.147.25 on 27/08/2024 at 12:11

Numerical simulation and experiment of error field measurement using luminous trace of electron beam in SST-1

Someswar DUTTA¹, Y PARAVASTU¹, J DHONGDE¹, H CHUDASMA¹,
S GEORGE¹, K DHANANI¹, A MAKWANA¹, C DODIYA¹, P VARMORA¹,
D K SHARMA¹, A K SINGH¹, U KUMAR¹, D RAVAL¹, U PRASAD¹, Z KHAN¹,
R SRINIVASAN^{1,2} and D RAJU¹

¹ Institute for Plasma Research, Gandhinagar, Gujarat 382428, India

² Homi Bhabha National Institute (HBNI), Anushaktinagar, Mumbai 400094, India

E-mail: sdutta@ipr.res.in

Received 24 April 2019, revised 11 June 2019

Accepted for publication 12 June 2019

Published 23 July 2019



CrossMark

Abstract

In contrast to the earlier experiments conducted in other machines, here, in SST-1 the error field measurement experiment is performed with a filled gas pressure $\sim 8 \times 10^{-4}$ mbar which helped to create a luminescent toroidal beam of electron path originated due to impact excitation and guided by the toroidal magnetic field. Beam path deviations are observed and recorded from radial and top ports using visible range cameras. Such creation and detection of the electron beam path differs from the earlier works where the gun emitted electron beam deviation in ultra-high vacuum was detected on a collector-grid/fluorescent screen. In the present experiment, large beam deviations were observed. Later investigation of the experimental set-up reveals existence of a possible source of radial electric field in between the source and the vacuum vessel which are separately grounded. Thus, to understand the observed phenomena, experiments are numerically modeled with deviated TF coil set, PF coil set and the electron source location. A particle tracing code is used to follow the electron path in the magnetic field generated by the coil set of interest. Simulation results suggest that the large deviation corresponds to the $\mathbf{E} \times \mathbf{B}$ drifts and not due to the large field errors. Toroidally averaged field errors of the SST-1 TF coils at toroidal field of $B_0 = 15$ kG are negligibly small $\sim B_0 \times 10^{-6}$ or less, which should not adversely affect the plasma performance.

Keywords: electron beam, error field, SST-1, TF coil

(Some figures may appear in colour only in the online journal)

1. Introduction

In a tokamak, inaccuracies in fabrication and assembly of magnetic field coils produce asymmetry in the magnetic topology inside the device, such irregularities in the magnetic field are termed as inherent error-fields [1, 2]. Sources of inherent error fields in individual tokamaks are versatile in nature. The discreteness of the toroidal field coil system in any tokamak produces toroidal field ripple [3–6] which is an inherent field error in a tokamak. Such TF ripples have deleterious effects on particle confinement in tokamaks. Other

than that, the main sources of error fields are irregularities in coil shapes, positioning during assembly of the coil system and current feeders termed as bus bars which are the sources of highly asymmetric error fields. Error fields in a magnetic fusion device adversely affects plasma start-up, stability, and confinement [7]. If the error fields are not corrected properly, it may lead to plasma disruptions as well. Therefore, error fields in a tokamak have to be measured and corrected with suitable externally applied magnetic fields [8, 9]. Field errors are estimated either component/mode wise [1, 8–11] or as a toroidally averaged quantity [12–17]. The mode analysis of

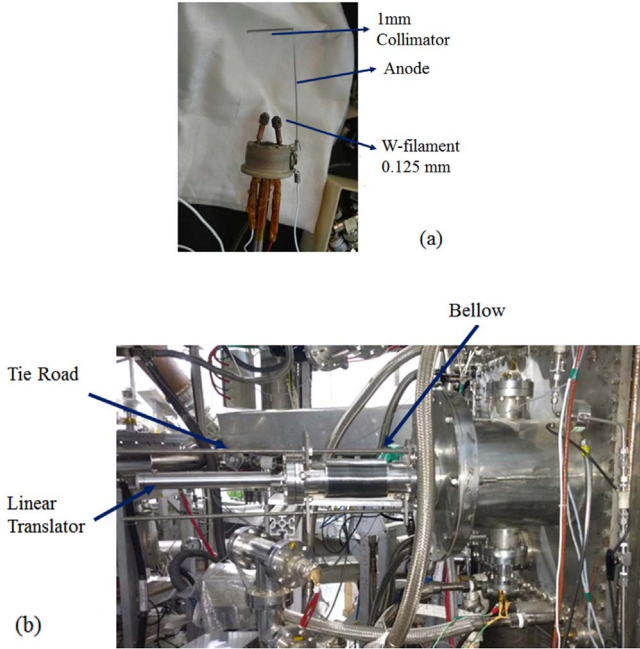


Figure 1. (a) Electron gun assembly consisting of tungsten filament and anode plate, (b) electron gun system integrated to the SST-1 Tokamak vessel.

error fields gives more insight to the error field distribution over the plasma surfaces and is a very important topic of tokamak research. However, in the present work, only toroidally averaged field errors arising from assembly errors of a TF coil system alone are estimated to explain the experimental observation in the SST-1 tokamak [18]. Error field measurements using electron beam source inside tokamak vessel is an established technique and has been used in several tokamaks around the globe [12–17]. An electron beam with only parallel energy along the toroidal magnetic field will follow the toroidal field with a curvature drift associated with this parallel energy. By subtracting the beam deviation due to curvature drift from the measured beam deviation, one can estimate the inherent error-field in the system. Such experiments have been carried out in EBT [13, 14], TEXTOR [15], KSTAR [16] and BETA (Basic Experiments in Toroidal Assembly) [17], to measure the inherent field errors associated with the various coil systems. In EBT and KSTAR, experiments were carried out with ultra-high vacuum vessel where the deviation of the electron beam originated from the gun was detected on a collector-grid or fluorescent screen. Here in BETA and SST-1, a different method has been adopted to trace the toroidal field with a visual toroidal beam created by electrons. In the experiment performed in SST-1, the filled gas pressure in the vacuum vessel is kept $\sim 8 \times 10^{-4}$ mbar, to create a luminescent toroidal beam of electron path guided by the toroidal magnetic field originated due to impact excitation. Beam deviation is recorded by visual range cameras mounted on the ports. It is a much easier method to trace the deviated beam path unlike the previously conducted experiments where a much more sophisticated and complicated experimental set-up is required. Thus, this method is more suitable for error-field estimation experiments

which are planned to be conducted in future reactors. Superconducting coil system of the SST-1 [18] tokamak consists of 9 poloidal field (PF) coils and 16 toroidal field (TF) coils. Both TF and PF coil systems have been assembled and the positional inaccuracies after the assembly of each individual coil are measured. So far, the TFC system was cooled to 4.5 K and charged to produce 25 kilo-Gauss (kG). Experiments have been carried out using only TF coils at room temperature and at 4.2 K, to find the irregularities in the toroidal magnetic field topology and corresponding fields at $R_0 = 110$ cm are 78 G and 15 kG. An attempt is made to compare experimental observation of electron beam deviation while it travels toroidally in the presence of a toroidal field with the numerical simulation of a test particle moving in the presence of electric and magnetic fields. The numerical simulation is used to derive the estimation of error field associated with the TF system of SST-1 tokamak using measured positional deviation of the beam [19]. Section 2 describes the experimental set up and observation of the experiments conducted. Section 3 describes the numerical modelling of the experiments and simulation results. In section 4, the summary and conclusions are described.

2. Experimental setup and observation

As mentioned earlier, electron beams have been used to study the magnetic topology in many tokamaks where they have kept the vacuum vessel in an ultra-high vacuum regime, whereas in the SST-1 experiment, the electron beam led visible beam originated due to atomic processes as it travels toroidally with filled pressure 8×10^{-4} mbar being used as the field line tracer. Thus this technique does not require any electron detectors to measure the beam deviation which reduces the complexity to carry out similar type of experiments.

2.1. Description of the system

A tungsten filament of 0.0125 cm length is used to emit electrons as shown in figure 1(a), where the anode is biased with 90–135 V to accelerate those emitted electrons which are then collimated by 0.1 cm aperture. The acceleration voltage range used here is chosen experimentally to form the visual toroidal beam.

Figure 1(b) shows the assembly of electron guns which consists of edge welded bellow, linear translator and tie rod. These are the main mechanical components which helped to move the electron gun setup from $R = 95$ cm to $R = 135$ cm with respect to the machine axis. Edge welded bellow used in the setup has a stroke length of 40 cm i.e. elongated length of 50.6 cm and compressed length of 9.9 cm and has a lateral offset of 0.5 cm. Edge welded bellow is used for coarse movement of electron gun setup with an accuracy of ~ 0.2 cm, as the pitch of M10 tie rod is 0.1750 cm. Linear translator used in the setup is for fine movement of electron gun setup. It has a stroke length of 15 cm with an accuracy of 0.01 cm. Tie rod on the setup is used to keep the bellow supported across its compressed and elongated length, and to keep the electron gun setup straight across the stroke length of 40 cm.

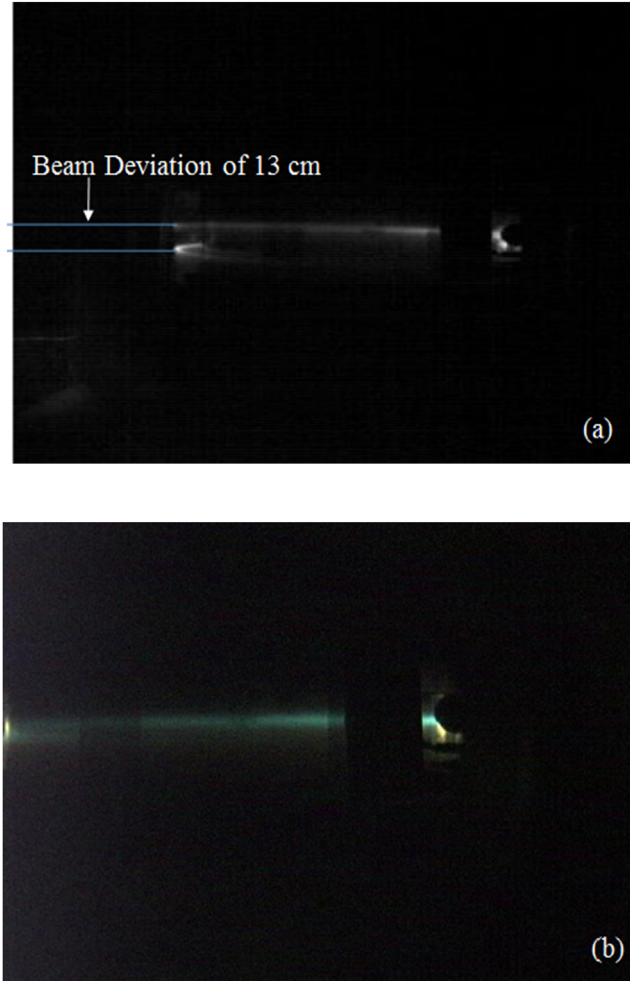


Figure 2. (a) Beam splitting of ~ 13 cm observed for $B_0 = 78$ G and accelerating voltage of 130 V case, (b) merger of the splitted beam with RCC switched on for $B_0 = 78$ G and accelerating voltage of 130 V case.

2.2. Experimental setup

In the SST-1 tokamak (major radius, $R_0 = 110$ cm and minor radius $a = 20$ cm), the above mentioned electron beam source is mounted on the radial port at the mid-plane to perform the experiment. A luminescent toroidal beam is created due to the impact excitation of helium gas by the electrons in the vacuum vessel. Such creation of luminescent beam of electron path differs from the method used earlier in EBT, T15, TEXTOR and KSTAR where the electron beam deviation in ultra-high vacuum was detected on a collector-grid/fluorescent screen. The gun emitted electrons constitute $\sim 10\text{--}20$ mA current. These emitted electrons would make $\sim 10^7$ numbers of excitations in one toroidal rotation so that enough luminescence exists to trace the path of the electrons. It is a new approach to trace the deviated beam path in contrast to previously conducted experiments where a much more sophisticated experimental set-up is required. Unlike other electron gun experiments mentioned earlier [1–4], in this case, the accelerating voltage floats by nature which means that the vessel and electron gun are separately

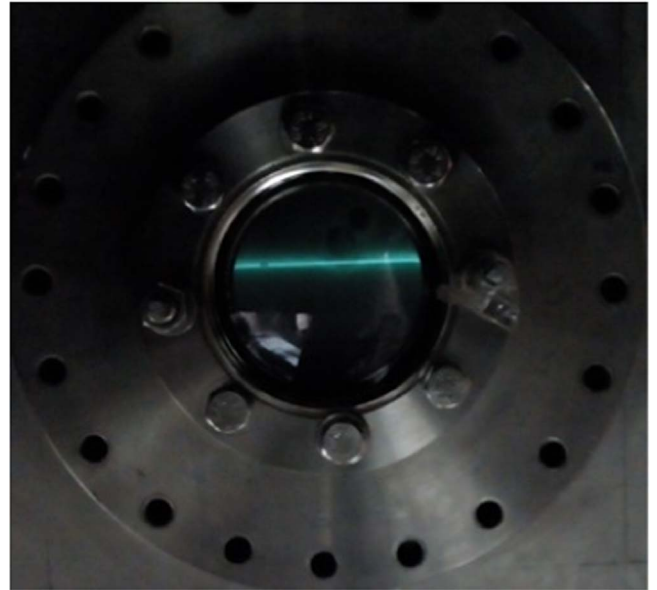


Figure 3. Luminescent beam at $R = 100$ cm does not split for $B_0 = 15$ kG case.

grounded and the direction of the electron beam is not perfectly aligned with the toroidal field tangent at the electron gun location. For these two reasons, a radial electric field will be generated which then imparts a perpendicular energy to the electrons. Therefore in this case, the $\mathbf{E} \times \mathbf{B}$ drift, grad- \mathbf{B} drift along with the curvature drift [20] has to be considered while estimating the inherent error-field of TFC from the measured beam deviations. Beam deviations are observed and recorded by visible range cameras mounted in the top and the radial port. Beam deviations are quantified by the image processing of the recorded footage from the camera. In this method, only the electron gun has to be mounted inside the vessel and rest of the system consists of non-intrusive components, thus the method will be very useful in future reactor devices.

2.3. Experimental observations

First set of experiments was performed with a TF input current of 25 A which corresponds to $B_0 = 78$ G of toroidal field at major radius $R_0 = 110$ cm. It is the maximum conductor current in TF coil that can be passed at room temperature. Beam emitter located at $R = 100$ cm where $B_T \sim 90$ G and electrons are accelerated within the range of 90–135 V. With this experimental set-up, beam line splitting of 13 cm to 20 cm has been observed, as shown in figure 2(a).

A pair of up-down symmetric coils to produce vertical fields named as radial control coils (RCC) of radius 138 cm located at $(0, 0, Z = \pm 37.8$ cm) is also used during this experiment. When RCC is switched on with ~ 200 A, the splitted beams merged together, as shown in figure 2(b).

In another set of experiments, when the TF coil is cooled to 4.2 K, about 4.8 kA current is passed through the single TF winding pack to produce ~ 15 kG toroidal magnetic field at R_0 . In this case, no beam splitting was observed with the same beam emitter location $R = 100$ cm and with accelerating voltage of 135 V, see figure 3.

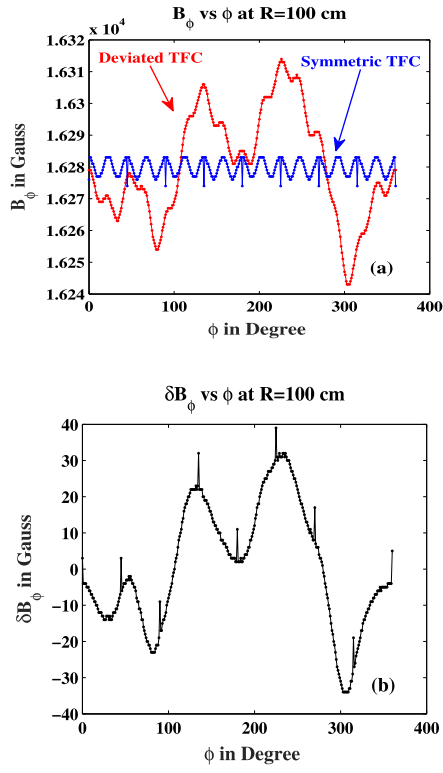


Figure 4. (a) B_ϕ versus ϕ at $R = 100$ cm for $B_0 = 15$ kG case, (b) δB_ϕ versus ϕ for $B_0 = 15$ kG case shows there is maximum of $\delta B_\phi \sim \pm 30$ G.

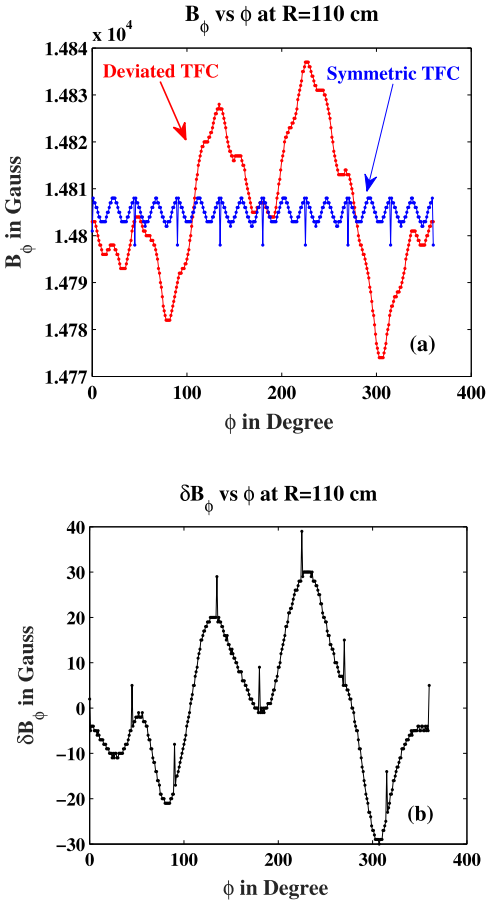


Figure 6. (a) B_ϕ versus ϕ at $R_0 = 110$ cm for $B_0 = 15$ kG case, (b) δB_ϕ versus ϕ at $R_0 = 110$ cm for $B_0 = 15$ kG case shows there is a maximum of $\delta B_\phi \sim \pm 30$ G.

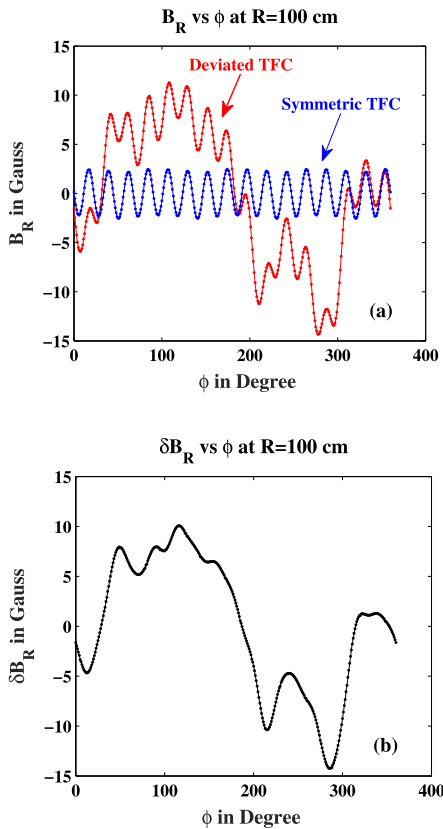


Figure 5. (a) B_R versus ϕ at $R = 100$ cm for $B_0 = 15$ kG case, (b) δB_R versus ϕ at $R = 100$ cm for $B_0 = 15$ kG case shows there is maximum of $\delta B_R \sim \pm 10$ G.

3. Numerical modeling of the experiment

In order to have a better understanding of observed beam deviations, experiments are modeled numerically to simulate the process as discussed in section 2.3. EFFI code [21] which can compute magnetic field, inductance and the forces for a given coil has been used to numerically model and analyze the TF coils. Any coils that can be constructed by arcs and straight current elements can be numerically modeled in EFFI and the corresponding fields can be computed as per the requirement. First, all 16 TFC as per design are numerically modeled and analyzed by EFFI code. Later field errors are estimated by incorporating positional deviations in cylindrical coordinate system: radial (R), azimuthal (ϕ) and vertical (Z) directions measured after assembly of the TFC system of SST-1. Field components produced by these as designed symmetric coil set and as assembled deviated coil set are numerically computed and then compared to estimate error-fields discussed in section 3.1. Finally, the deviated TFC model is used for numerical modeling of the experiment as detailed in section 3.2.

3.1. Numerical estimation of error fields for deviated TF coils due to misalignment during assembly of the SST-1 tokamak

A systematic study has been made to numerically estimate the error-fields in all three dimensions associated with the toroidal

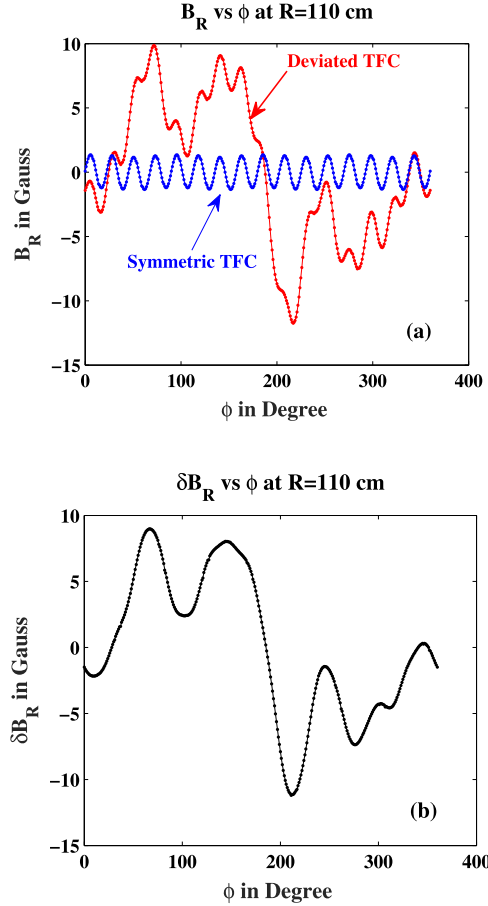


Figure 7. (a) B_R versus ϕ at $R_0 = 110$ cm for $B_0 = 15$ kG, and (b) δB_R versus ϕ at $R_0 = 110$ cm for $B_0 = 15$ kG shows that there is maximum of $\delta B_R \sim \pm 10$ G.

field coil deviations arising from the misalignment during the assembly of the same. There is no difference in the B_z field and it is zero for all toroidal angle for both symmetric and deviated TF coil sets. Thus, there is no B_z error field associated with these deviations. Three radial positions are chosen to analyze the radial variation of error-field components. Difference in B_R and B_ϕ components δB_ϕ and δB_R along ϕ direction at probe location $R = 100$ cm, at the major radius $R = 110$ cm and at the plasma edge $R = 130$ cm, $Z = 0$ cm for only $B_0 \sim 15$ kG case with and without deviations are plotted in figures 4–9.

The maximum amplitude of the error-field δB_ϕ increases towards the outboard side along the major radius, as seen in figures 4, 6 and 8, similar patterns are observed for δB_R , see figures 5, 7 and 9. The average of these error-fields δB_R and δB_ϕ over one toroidal transit will have very small amplitudes which would affect the electron orbit slightly for lower toroidal fields. The ratios of $\delta B_R/B_0$ and $\delta B_\phi/B_0$ averaged over one toroidal transit are of the order of $\sim 10^{-6}$, which are quite small field errors as observed in other tokamaks in the world; thus, it would not pose any serious threat to the plasma operations in the SST-1.

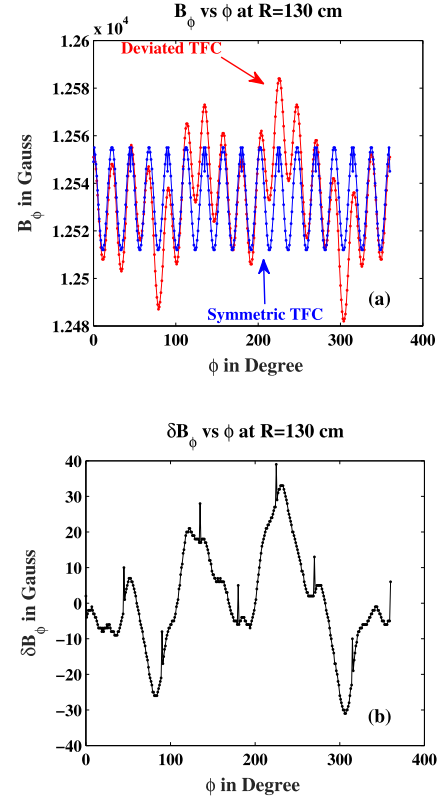


Figure 8. (a) B_ϕ versus ϕ at $R = 130$ cm for $B_0 = 15$ kG, and (b) δB_ϕ versus ϕ at $R = 130$ cm for $B_0 = 15$ kG shows there is a maximum of $\delta B_\phi \sim \pm 30$ G.

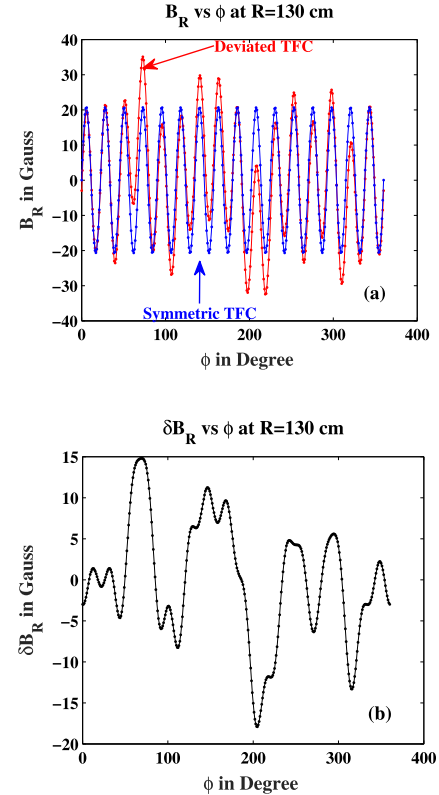


Figure 9. (a) B_R versus ϕ at $R = 130$ cm for $B_0 = 15$ kG, and (b) δB_R versus ϕ at $R = 130$ cm for $B_0 = 15$ kG shows there is maximum of $\delta B_R \sim \pm 15$ G.

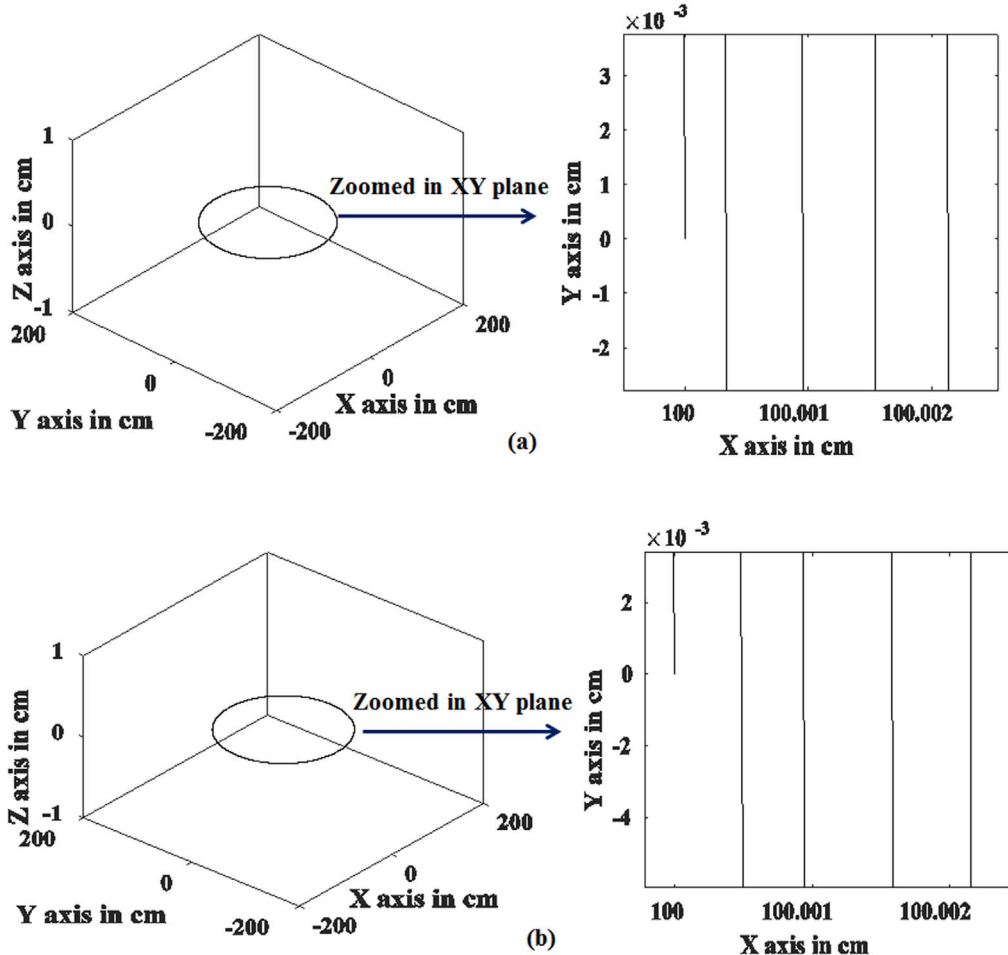


Figure 10. (a) Toroidal field lines traced at $R = 100$ cm for $B_0 = 78$ G. Small line splitting observed in XY plane suggests existence of very small radial error field, (b) toroidal field line traced at $R = 100$ cm for $B_0 = 15$ kG. Small line splitting observed in XY plane suggests existence of very small radial error field.

3.2. Modeling of the error field experiment using deviated TF coils of SST-1

Field line tracing for the deviated TFC system (as assembled) shows no field line opening in the Z -direction as shown in figures 10(a) and (b) for two toroidal fields of 78 G and ~ 15 kG at R_0 , which could not explain the 13–20 cm beam deviations observed in the experiment, see figure 2(a). It means there is no or negligibly small B_z error field associated with those TF coil deviations. Radial field variations causes very small $\sim 10^{-3}$ cm broadening of the field lines in the radial direction (x -axis), as shown in the respective zoomed figure. Such radial broadening $\sim 10^{-3}$ cm corresponds to a toroidally averaged radial error field $\delta B_R \sim B_0 \times 10^{-6}$, using the formula given in [16].

As mentioned earlier, there could be perpendicular energy sources due to the floating ground and improper alignment of the electron gun. A test particle model with grad- \mathbf{B} , curvature drift and an $\mathbf{E} \times \mathbf{B}$ drift is developed to study the experiment. It is found that different proportions of perpendicular and parallel energy of test particles can give a total deviation of few tens of cm in one toroidal rotation. In

this simulation total energy of 130 eV is shared equally in the parallel and perpendicular directions and a uniform \mathbf{E} field of $130/d$ V/cm, where $d = 20$ cm is considered as the distance of the nearest conducting wall of the vessel from the beam emitter to model the floating potential between them. A test particle code that takes the ideal toroidal field as a function of $(1/r)$ and uses Lorentz force to trace the particle orbit is used to model these experiments. Numerical simulations of the experiment with the assumption of the uniform floating \mathbf{E} field as mentioned earlier, produces beam deviation of the same order as observed in the experiment. Later this test particle code is integrated as a module (PARTICLE) with the EFFI code to use the actual magnetic field data for the symmetric and deviated TF coil configuration of SST-1 to give the realistic estimation of the drifts and the error fields in both R and Z directions. Simulation for the experiment with $B_0 = 78$ G with the developed EFFI module gives a gyro-center (GC) deviation of ~ 13 cm as shown in figure 11(a) below. Both particle orbit and the GC path have been shown at an angle $\sim 200^\circ$ from the beam emitter in figure 11(a) and the whole orbit of the electron with its guiding center is depicted in figure 11(b).

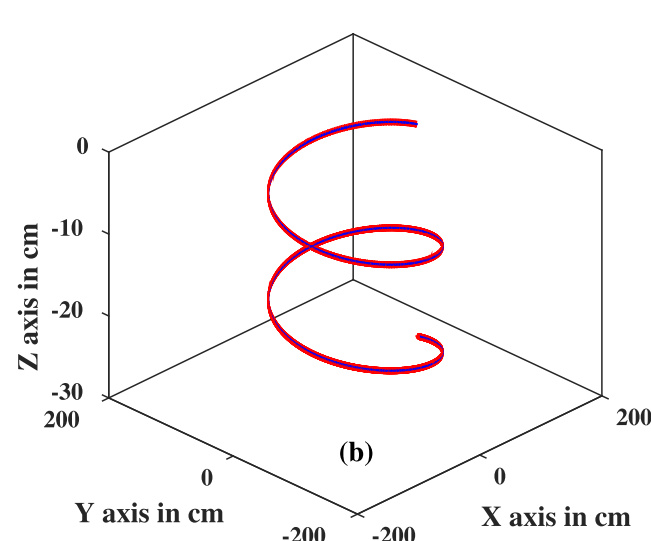
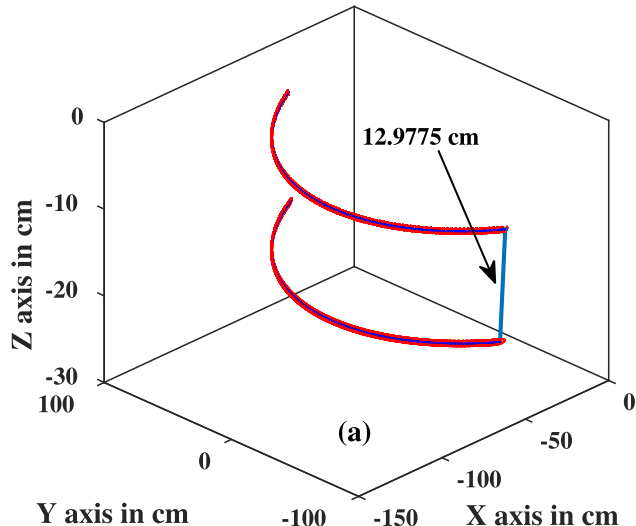


Figure 11. (a) $B_0 = 78$ G case, beam deviation of ~ -13 cm is observed from the port location. (b) $B_0 = 78$ G case, electron orbit/beam path for 2 toroidal transit.

In figure 12 the merger of the splitted beam is depicted when RCC is switched on with a current of around 200 A that produces $B_z \sim -1.89$ G at $R = 100$ cm. The RCC produced B_z field has compensated the electron drifts.

Another simulation for the $B_0 \sim 15$ kG at $R_0 = 110$ cm and the beam emitter located at $R = 100$ cm with 135 V accelerating potential has been carried out and the corresponding E field. In this case, the parallel velocity is kept twice so that the perpendicular component can trace the electron toroidally quickly; this will increase the curvature drift and will not affect the other drifts. The simulation result shows that the electron beam path has a negligible deviation of the order of $\sim 10^{-2}$ cm for 1 toroidal transit, thus, seen as a single line from the port location; see figures 13(a) and (b).

This is in agreement with the experimental observation as shown in figure 3, where the parallel energy was even less than the simulated case. Therefore it is confirmed that the

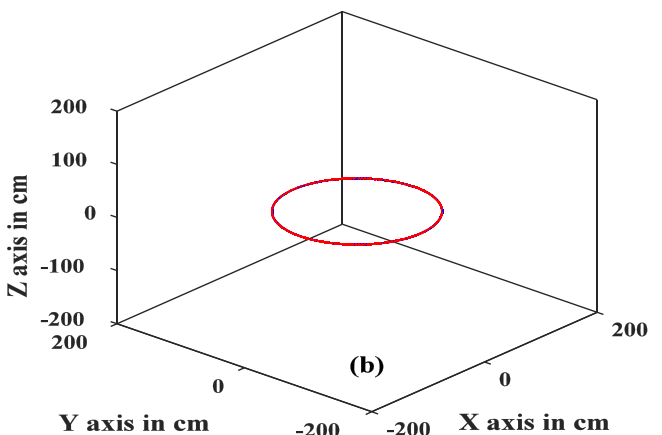
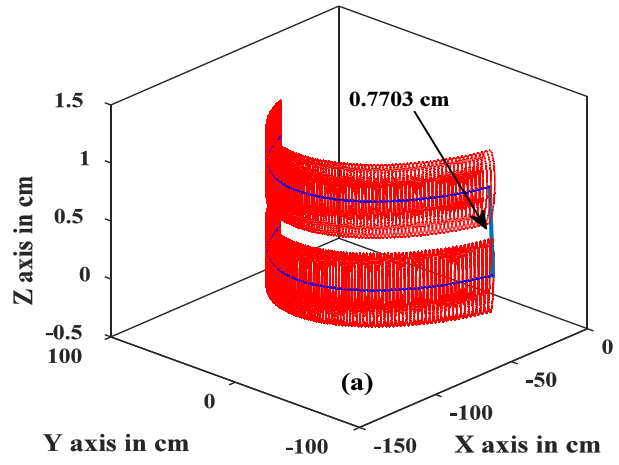


Figure 12. (a) $B_0 = 78$ G case with RCC switched on, beam deviation of ~ 0.8 cm zoomed view, (b) $B_0 = 78$ G case electron orbit for 2 toroidal transit are very close to each other that they would be seen as single line from the port.

beam deviation of 13 cm for the $B_0 = 78$ G case was due to the $\mathbf{E} \times \mathbf{B}$ drift arising from the \mathbf{E} field which originated from the integration of beam sources with the vessel of SST-1, and not due to the B_z error field associated with TF coil deviations.

4. Summary and conclusion

Error-field measurement experiments are approximately modeled by the EFFI code along the PARTICLE module to trace electron orbit in the deviated TF coil system of SST-1. Simulation results showed close proximity to the experimentally observed phenomena of beam deviation of the same order for the $B_0 = 78$ G case considering electron drifts of three types mentioned in the last section. When the toroidal field is much higher, $B_0 \sim 15$ kG both in the experiment and in the simulation results, no significant beam deviation is observed. Thus, it is confirmed that the beam deviation observed for the lower field $B_0 = 78$ G case is due to the phenomena of particle drift and not due to the B_z error field

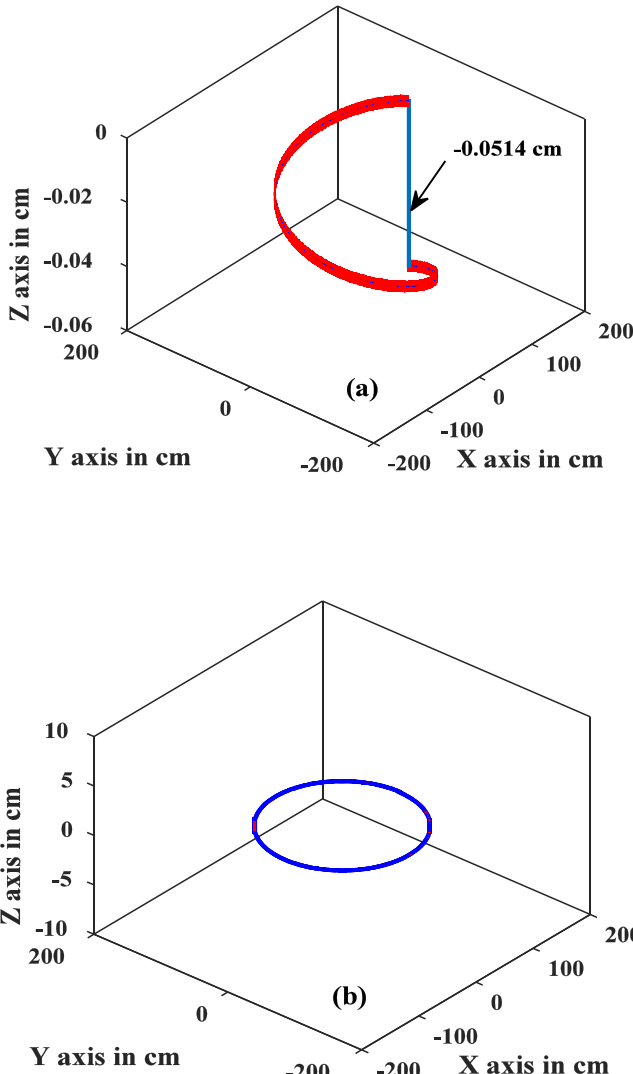


Figure 13. (a) $B_0 \sim 15$ kG case, beam deviation of $\sim 10^{-2}$ cm zoomed view. (b) $B_0 \sim 15$ kG case, electron orbit for 1 toroidal transit, with more toroidal transit also it would be seen as single line from the port.

associated with the TF coil system. The fact is again supported by the component analysis of toroidal field B_T in R , ϕ and Z direction as described in section 3.1, which confirms there is no δB_z associated with the deviated TF coil system. With very small amounts of average $\delta B_R/B_0 \sim 10^{-6}$, the field lines are radially shifted with each toroidal transit by 10^{-3} cm, as shown in figure 10. The effect of error field in the toroidal direction δB_ϕ can be associated to the increased localized

toroidal field ripple by 0.1% where the peak of the δB_ϕ is located toroidally, see figures 4, 6 and 7. Therefore no significant toroidally averaged error field is associated with the SST-1 TF coil system as supported by both experimental and simulation results. However, the existence of the toroidal field error in combination with the radial field error may give rise to the error fields of low toroidal mode on the plasma surface.

Acknowledgments

Authors wish to acknowledge the contribution of other colleagues from the SST-1 team. Also, the author wishes to thank Mr H L Swami for his continuous support and encouragement in completing the article.

References

- [1] Scoville J T and La Haye R J 2003 *Nucl. Fusion* **43** 250
- [2] Tan H et al 2014 *Fusion Sci. Technol.* **65** 406
- [3] Tobita K et al 1995 *Nucl. Fusion* **35** 1585
- [4] Portone A et al 2008 *Fusion Eng. Des.* **83** 1619
- [5] Liu S L et al 2013 *Fusion Eng. Des.* **88** 675
- [6] Liu S L et al 2009 *Fusion Eng. Des.* **84** 1206
- [7] La Haye R J et al 1992 *Phys. Fluids B* **4** 2098
- [8] Park J-K et al 2008 *Nucl. Fusion* **48** 045006
- [9] Leuer J A et al 1998 *Proc. Symp. Fusion Technology* (Marseille, France 1998) p 513 (<https://fusion.gat.com/pubs-ext/SOFT98/A22920.pdf>)
- [10] Butterly R J et al 1999 *Nucl. Fusion* **39** 1827
- [11] Rao B et al 2013 *Rev. Sci. Instrum.* **84** 043504
- [12] Colchin R J et al 1989 *Rev. Sci. Instrum.* **60** 2680
- [13] Uckan T 1985 *Rev. Sci. Instrum.* **56** 90
- [14] Owen L W et al 1983 *Proc. Advanced Bumpy Torus Concepts Workshop CONF-830758* (Oak Ridge, TN: Oak Ridge National Laboratory) 55
- [15] Neubauer O et al 1997 *ANS Fusion Technol.* **31** 154
- [16] England A C et al 2011 *Fusion Eng. Des.* **86** 20
- [17] Thatipamula S G et al 2015 *Rev. Sci. Instrum.* **86** 033504
- [18] Saxena Y C and Team SST-1 2000 *Nucl. Fusion* **40** 1069
- [19] Dutta S et al 2018 Error Field Experiment and Analysis in SST-1 27th IAEA FEC—IAEA CN-258 Gandhinagar India 22-27 October FIP/P7-19 (<https://conferences.iaea.org/indico/event/151/contributions/6158/contribution.pdf>)
- [20] Chen F F 1984 *Introduction to Plasma Physics and Controlled Fusion V. 1 Plasma Physics* 2nd edn (New York: Plenum Press)
- [21] Sackett S J 1978 EFFE: A code for calculating the electromagnetic field, force, and inductance in coil systems of arbitrary geometry LLNL Livermore California UCRL-52402 (<http://inspirehep.net/record/130169?ln=en>)